Nuclear Architecture and Patterns of Molecular Evolution Are Correlated in the Ciliate *Chilodonella uncinata*

Xyrus X. Maurer-Alcalá[1,2] and Laura A. Katz[1,2,*]

[1]Department of Biological Sciences, Smith College, Northampton, MA

[2]Program in Organismic and Evolutionary Biology, University of Massachusetts Amherst, Amherst

*Corresponding author. E-mail: lkatz@smith.edu.

Abstract

The relationship between nuclear architecture and patterns of molecular evolution in lineages across the eukaryotic tree of life is not well understood, partly because molecular evolution is traditionally explored as changes in base pairs along a linear sequence without considering the context of nuclear position of chromosomes. The ciliate *Chilodonella uncinata* is an ideal system to address the relationship between nuclear architecture and patterns of molecular evolution as the somatic macronucleus of this ciliate is composed of a peripheral DNA-rich area (orthomere) and a DNA-poor central region (paramere) to form a "heteromeric" macronucleus. Moreover, because the somatic chromosomes of *C. uncinata* are highly processed into "gene-sized" chromosomes (i.e., nanochromosomes), we can assess fine-scale relationships between location and sequence evolution. By combining fluorescence microscopy and analyses of transcriptome data from *C. uncinata*, we find that highly expressed genes have the greatest codon usage bias and are enriched in DNA-poor regions. In contrast, genes with less biased sequences tend to be concentrated in DNA abundant areas, at least during vegetative growth. Our analyses are consistent with recent work in plants and animals where nuclear architecture plays a role in gene expression. At the same time, the unusual localization of nanochromosomes suggests that the highly structured nucleus in *C. uncinata* may create a "gene bank" that facilitates rapid changes in expression of genes required only in specific life history stages. By using "nonmodel" organisms like *C. uncinata*, we can explore the universality of eukaryotic features while also providing examples of novel properties (i.e., the presence of a gene bank) that build from these features.

Key words: nuclear architecture, genome evolution, codon bias, in situ hybridization, Protist.

Introduction

Our understanding of the spatial organization of DNA in the interphase nucleus has changed dramatically over the past two decades, largely due to the myriad studies performed on mammalian cell lines (Cremer et al. 2001; Kupper et al. 2007; Tai et al. 2014). From this work, a model of the interphase nucleus has emerged where decondensed chromosomes are allocated to distinct nuclear regions (i.e., chromosome territories) that are delineated by chromatin poor (i.e., interchromatin) compartments. This chromosome territory-interchromatin compartment (CT-IC) model is now accepted as a major organizing principle of the interphase nucleus due to the widespread conservation of this architecture among animals (Cremer et al. 2001; Tanabe et al. 2002) as well as plants, though studies here are more limited (Fransz et al. 2002).

Studies of mammalian cells have shown that variation in the radial distribution of individual chromosomes are linked to the morphology of the nucleus itself (Sun et al. 2000; Cremer et al. 2001). For example, analyses of "flat" nuclei of fibroblasts reveal chromosomes that are radially arranged by their size such that large chromosomes are found surrounding shorter ones (Sun, et al. 2000; Cremer et al. 2001). In animal tissues with more spherical nuclei, chromosome distribution correlates best with gene density per chromosome: Gene-poor chromosomes, often rich in repetitive elements, are typically inactive as heterochromatin and tend to be situated close to the nuclear envelope (Akhtar and Gasser 2007). Gene-dense chromosomes remain euchromatic, occupying the nucleus' center (Kupper et al. 2007) and are closer to transcriptional foci than expected by chance, supporting the nonrandom distribution of chromosomes in the nucleus (Meister et al. 2010). Together, gene density and transcriptional activity likely regulate the position of entire chromosomes (Mahy et al. 2002). Although based predominantly

on a single lineage of eukaryotes, animals, this organization of heterochromatin surrounding a euchromatin core, coupled with the CT-IC model, has become the standard view of the eukaryotic nucleus.

There are few studies examining the nuclear architecture in lineages other than animals and plants, though examples of atypical chromosomes are known. Such examples include the variant surface glycoprotein genes found on mini-chromosomes in the parasitic trypanosome *Trypanosoma brucei* (Navarro et al. 2007), the crystalline chromosomes of dinoflagellates (de la Espina et al. 2005; Bachvaroff et al. 2014), and the fragmented and amplified chromosomes found in some ciliates (Prescott 1994; Postberg et al. 2005). Despite the presence of unusual chromosomes, Postberg et al. (2005) have suggested that aspects of the CT-IC model also exist in the ciliate *Stylonychia lemnae* and may be a common eukaryotic feature. The "gene-sized" nanochromosomes in *S. lemnae* form chromatin-dense regions, resembling chromosome territories, surrounded by a diffuse chromatin-poor network throughout the somatic macronucleus (Postberg et al. 2005).

Analyses of interactions between nuclear architecture and patterns of molecular evolution (i.e., changes in DNA sequences) are limited and also largely restricted to animal lineages. There is a well-documented relationship between high codon bias (i.e., strong selection on silent sites) and high levels of gene expression (Duret and Mouchiroud 1999; Duret 2002; Ma et al. 2014) but these studies generally do not assess the relationship to nuclear architecture. In *Drosophila*, gene family members residing in euchromatic regions are significantly more biased in codon usage than orthologous members in heterochromatic portions of the same chromosome (Diaz-Castillo and Golic 2007). Such euchromatic regions of chromosomes are typically found in closer proximity to areas of active transcription (Simonis et al. 2006), suggesting that nuclear architecture may reflect molecular evolution, at least in some animal lineages.

Taking advantage of the presence of nanochromosomes in the somatic macronuclei of *Chilodonella uncinata*, we address the relationship between nuclear architecture and genome evolution. Like other ciliates with extensively processed somatic chromosomes (e.g., the classes Spirotrichea and Armophorea), *C. uncinata* has a heterochromatin-rich germline micronucleus and a spherical macronucleus containing nanochromosomes that are highly and unevenly amplified (Radzikowski and Steinbruck 1990; Riley and Katz 2001; Bellec and Katz 2012; Huang and Katz 2014). Unlike other ciliates whose chromosomes are more diffusely arranged (Foissner 1996; Postberg et al. 2005), *C. uncinata* and some other members of the class Phyllopharyngea possess a heteromeric somatic macronucleus comprised of two distinct zones: 1) A DNA-rich perimeter (orthomere) consisting of dense chromatin granules close to the nuclear envelope and 2) a DNA-poor interior (paramere) with diffuse DNA (Pyne 1978; Bellec

et al. 2014). We combine fluorescent in situ hybridization methods and analyses of transcriptomic data to demonstrate the link between *C. uncinata*'s unusual nuclear architecture and patterns of molecular evolution.

Materials and Methods

Cell Lines and Culture

Chilodonella uncinata (Pol strain, ATCC PRA-257) was cultured in filtered and autoclaved pond water with a rice grain to support bacterial growth at room temperature and in the dark. Prior to fixation cells were collected from culture during exponential growth, centrifuged and then washed in sterile water.

Transcription Labeling

For pulse labeling of RNA synthesis, *C. uncinata* cells were incubated in filtered and autoclaved pond water containing 1 mM 5-ethynyl uridine (EU; Invitrogen) for 30 min directly on Superfrost microscope slide (Fisher). Cells were then fixed in 2% paraformaldehyde solution in phosphate buffer solution (PBS) for 30 min. Fixed cells were then washed in PBS and permeabilized with 0.5% Triton X-100 for 10 min at room temperature. EU labeling was carried out according to the manufacturer's instructions (Invitrogen; Click-iT RNA labeling kits). The cells were incubated in a 1× working solution of Click-iT reaction solution for 30 min at room temperature. Subsequently, the slides were washed once with Click-iT reaction rinse buffer then once more with PBS. Following this, DNA was counterstained with 0.1 μg/ml 4′,6-diamidino-2-phenyl-indole (DAPI) for 1 min in the dark. Cells were then washed twice with PBS and a drop of SlowFade Gold was added prior to sealing with nail polish.

Flourescence In Situ Hybridization

Localization of macronuclear α-tubulin, β-tubulin paralogs, and nSSU-rDNA genes was performed one at a time using oligonucleotide probes labeled at their 5′-ends with Alexa Fluor 488, 594, or 647. Probe sequences are as follows:

α-tubulin: 5′-GTCGTCGATGAGGTCAGAACCGGAACCTAC AGACAACTGTTCCAC-3′
β-tubulin P2: 5′-CGCGTGCAAGAGCGGTTTGTGGAACTGA TGCGGGTCCGGGCGTAC-3′
β-tubulin P3: 5′-GCAGTCTCGTACTCAAAGCAGCCAGTAG ATGGGAACCAAACCTCA-3′
nSSU: 5′-CGGAGAGGCTAGGGAACTTTAATCGGAACTCTA GATGACCCAGCA-3′

Cells were fixed directly onto slides as previously described. Cells were then permeabilized in 0.5% Triton X-100 in PBS for 20 min at room temperature, washed briefly with PBS, and incubated in 0.1 N HCl for 5 min at room temperature. Cells were treated with 100 μg/ml of RNase

One (NEB) for 1 h at 37 °C before being equilibrated overnight in a mix of 50% formamide in 2× SSC at room temperature. Oligonucleotide probes were dissolved in hybridization buffer (20% formamide, 4× SSC) with 50 ng/μl of unlabeled *Chilodonella* DNA. Denaturation of nuclear DNA was performed in 70% formamide/2× SSC at 75 °C for 5 min. The hybridization mix was denatured separately at 95 °C for 10 min, snap cooled in an ice bath, loaded onto slides, and incubated overnight at 37 °C in a moist incubator. Posthybridization washes were performed in 2×, 1×, and then 0.1× SSC at 42 °C. Nuclei were counterstained and sealed as described above.

Confocal Laser Scanning Microscopy

Cells were analyzed using a Leica TCS SP5 confocal laser scanning microscope equipped with an oil immersion 63/1.4 objective lens (HPX PL APO). Fluorochromes were visualized with an ultraviolet laser with an excitation wavelength of 405 nm for DAPI, an argon laser with an excitation wavelength of 488 nm for Alexa Fluor 488™, and helium-neon lasers with excitation wavelengths of 594 for Alexa Fluor 594™ and 633 for Alexa Fluor 647™. Images were scanned sequentially, generating 8-bit gray scale images. All images were captured with a resolution of 1,024 × 1,024 pixels, an acquisition speed of 200 Hz and a line average of 8 to reduce noise. ImageJ (Rasband, W.S., ImageJ, U. S. National Institutes of Health, Bethesda, MD; http://imagej.nih.gov/ij/, 1997-2014) was used to convert 8-bit gray scale images to false RGB colors and for image analysis.

Image Analysis

For each nanochromosome probe and transcription labeling, z-stacks of 50 nuclei that were determined to be most circular by eye were taken for radial measurements (i.e., in 30° increments) using ImageJ. Measurements of fluorescent intensity were taken from the slice with the greatest diameter and the fluorescence profile was taken from the center of the macronucleus toward the nuclear perimeter every 30°. Once all measurements were made, they were normalized against each macronucleus' maximal fluorescent intensity and radial distance (as the size of each macronucleus is variable depending on cell size) and then were averaged across all 50 nuclei before plotting.

Compositional Bias and Codon Usage

Calculations of Guanine-Cytosine content of third position 4-fold degenerate sites (GC3s) and the effective number of codons were done through the use of custom python scripts (available: https://github.com/maurerax/Basic-Informatics-Katzlab-). The analyses made use of the transcriptome assembly of the Pol strain of *C. uncinata* (Grant et al. 2012) and *Tetrahymena thermophila* (Miao et al. 2009).

Results and Discussion

Transcription Is Concentrated in Chromatin-Poor Areas

We used fluorescent microscopy to assess the distribution of RNA transcripts within the somatic macronucleus of *C. uncinata*. Such analyses must be interpreted in light of the heteromeric nature of the macronucleus in this ciliate: The thousands of somatic nanochromosomes are arranged into a DNA-rich peripheral orthomere and a DNA-poor central paramere. To detect newly synthesized RNA, we measured the incorporation of the uridine analog EU over a 30-min interval, revealing that the majority of transcripts accumulate in the central paramere as compared with the peripheral orthomere (fig. 1).

These analyses contrast with observations made by Radzikowski (1976), which suggested that transcription was greatest in the DNA-rich orthomere as compared with the paramere itself. An explanation for the difference in our findings and those observed by Radzikowski (1976) may be related to the choice of probes and overall technique: After incubation with radioactive uridine for "a long time," the rRNAs that are heavily transcribed likely provided the clearest signal in autoradiographic studies by Radzikowski (1976) occurring in nucleoli, which are often nestled in close proximity to the orthomere and the nuclear envelope (i.e., DNA-poor gaps near nuclear perimeter; figs. 1A and 2A). In contrast, our approach reveals the short-term accumulation of transcripts both in putative nucleoli and throughout the large DNA-poor paramere. Moreover, Radzikowski (1976) isolated only nuclei through additional manipulations that altered the morphology of macronuclei (i.e., fig. 7 and 8 in Radzikowski 1976), which may also contribute to differences between the studies.

Transcriptional activity corresponds to nuclear architecture in diverse eukaryotes, although the heteromeric nature of nuclei is unique to ciliates within the class Phyllopharyngea (Raikov 1982; Hausmann and Bradbury 1996). In lineages such as animals and plants, transcriptionally active regions of chromosomes are either recruited to DNA-poor foci of intense transcription (e.g., transcription factories) or near nuclear pores, facilitating rapid exportation of nascent RNAs (Straatman et al. 1996; Pombo et al. 1997). In *C. uncinata*, there is a large transcriptional neighborhood lacking the distinct foci typical of transcription factories, suggesting that the small size and high abundance of nanochromosomes make transcription factories unnecessary in *C. uncinata*.

Distinct Organization of Somatic Nanochromosomes

We investigated the spatial distribution of specific nanochromosomes within the heteromeric macronucleus of *C. uncinata*. Using Oligo-FISH (flourescence in situ hybridization; Zwirglmaler et al. 2003), we captured the spatial distribution of nSSU-rDNA and three protein-coding nanochrosomes using 45-mer probes. Two of these genes, nSSU-rDNA and α-tubulin, represent at least an order of magnitude
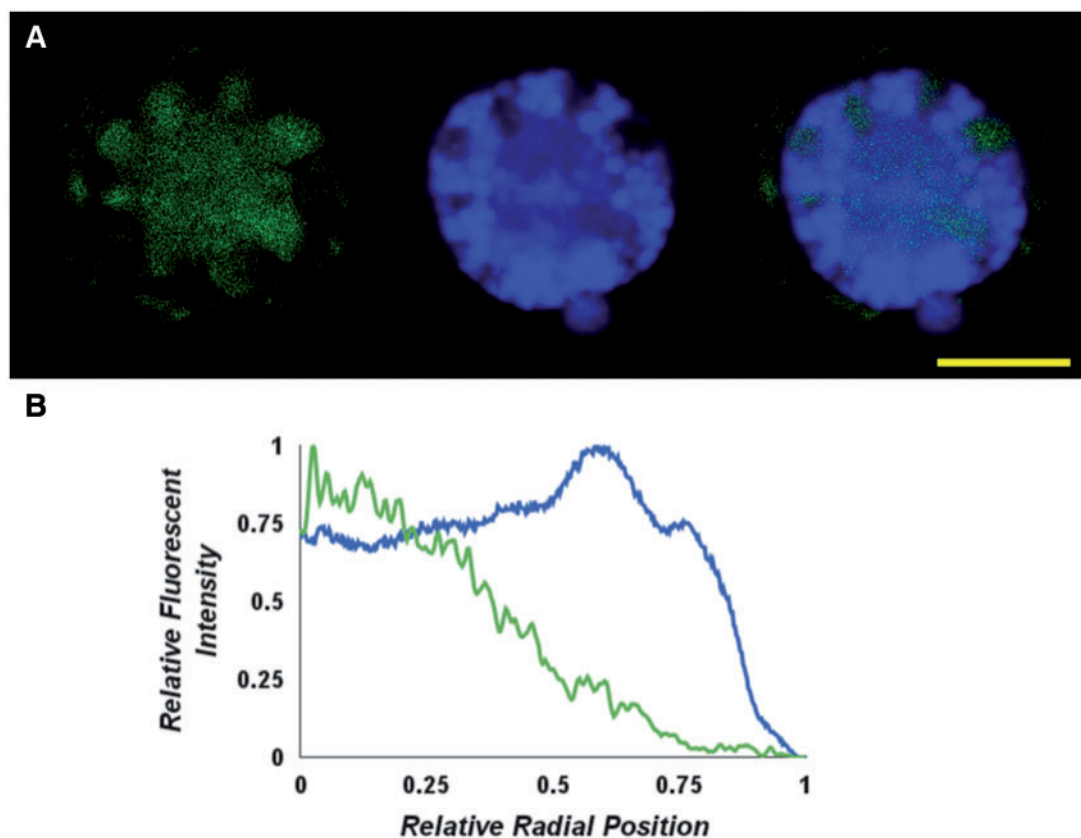
FIG. 1.—RNA (green) transcription is predominantly found in the DNA-poor regions of the macronucleus (blue), including nucleoli, as measured from the macronuclear center to the nuclear envelope. (A) Location of transcripts determined with "click" chemistry (green, RNA; blue, DAPI; yellow, overlay). Scale bar: 5 μm. (B) Distribution of fluorescent intensity estimated radially in 30° increments for each nucleus and averaged over 50 cells. Green, nascent RNA; blue, DNA. .

difference in nanochromosome copy number (5.9×10^4 and 8.5×10^3 copies, respectively) and relative expression (5.6×10^5 and 1.3×10^3 transcripts, respectively) as estimated from qPCR analyses (Bellec and Katz 2012; Huang and Katz 2014). The other two genes, paralogs P2 and P3 of β-tubulin, share similar nanochromsome copy numbers (6.4×10^4 and 3.2×10^3 copes, respectively) to the two highly expressed genes, yet have no measureable transcription during vegetative growth (Bellec and Katz 2012; Huang and Katz 2014).

The distribution of highly expressed nSSU-rDNA and α-tubulin nanonchromosomes is distinct from the lowly expressed β-tubulin paralogs P2 and P3. The highly expressed nSSU-rDNA nanochromosomes are found enriched in the paramere as well as in putative nucleoli nestled within the orthomere (fig. 2A), while highly expressed α-tubulin nanochromosomes have a more uniform distribution throughout the entire macronucleus (fig. 2B). In contrast, both of the lowly expressed β-tubulin paralogs are restricted to the orthomere of the macronucleus (figs. 2C and D), with almost no fluorescent signal measureable in the DNA-poor paramere during vegetative growth. Quantifying the distribution of nanochomosomes along the macronuclear radius (i.e., from macronuclear center to envelope), we show that highly expressed nanochromosomes are significantly enriched in the paramere compared with the lowly expressed β-tubulin paralogs (figs. 2 and 3). The relationship between the distributions of nanochromosomes is related to the distinct localization of transcription described above. Both of the lowly expressed nanochromosomes (β-tubulin P2/P3) are enriched in the DNA-rich orthomere near the nuclear envelope where transcription appears absent (figs. 2C, 2D, 3C, 3D).

Despite the differences in genome architecture among eukaryotic lineages (i.e., the unique heteromeric arrangement in *C. uncinata*), the recruitment of highly expressed genes to DNA-poor regions appears common across eukaryotes (Osborne et al. 2004; Postberg et al. 2006; Navarro, et al. 2007). Postberg et al. (2006) found α-tubulin nanochromosomes in close proximity to DNA-poor areas, presumably transcriptionally active, in the somatic nucleus (i.e., macronucleus) of the ciliate *S. lemnae*. Similarly, highly expressed genes in *C. uncinata* are found in the DNA-poor paramere (figs. 2 and 3), presumably a means for ensuring that these genes are
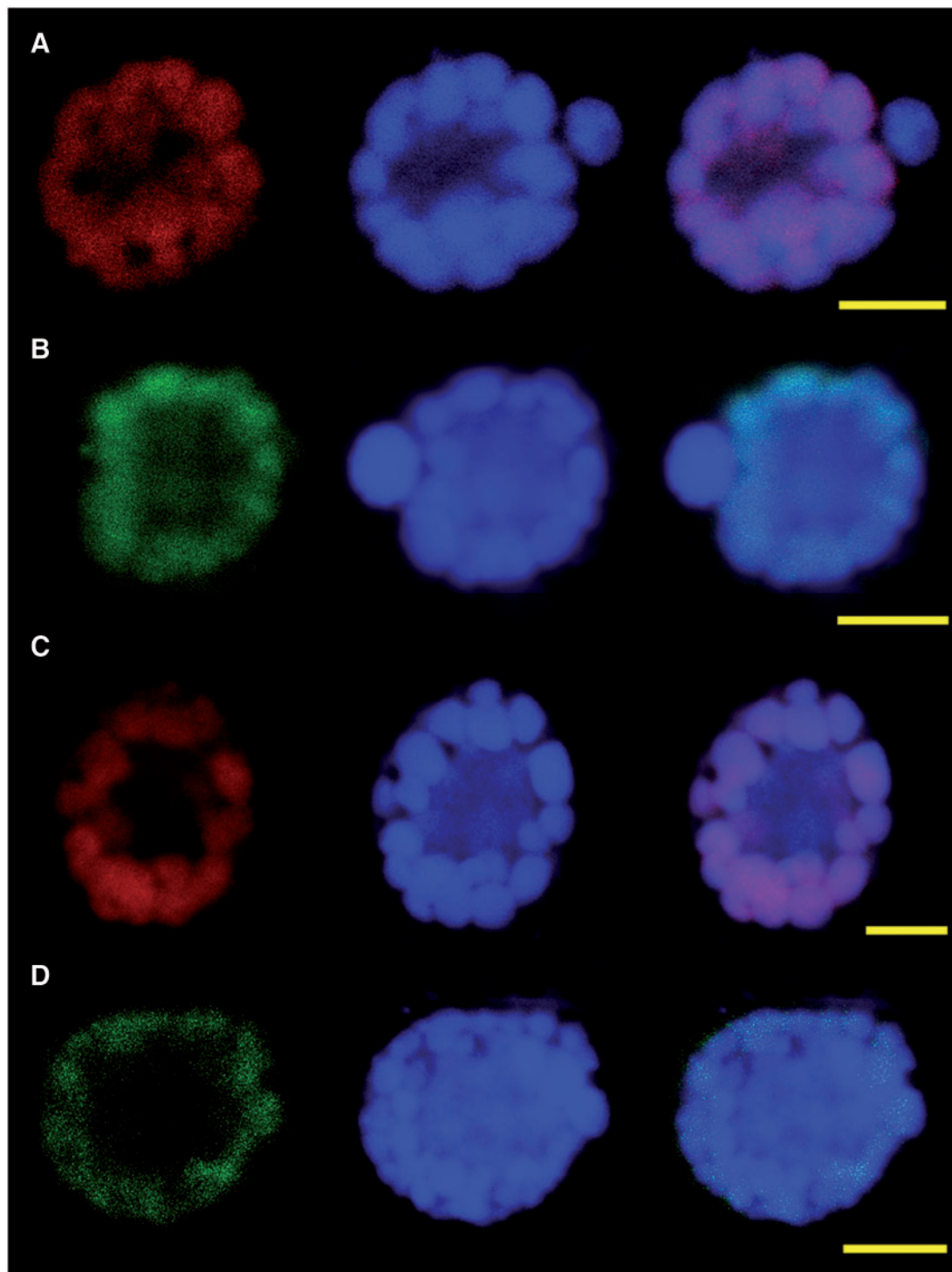
FIG. 2.—Nanochromosomes are distributed nonrandomly and in distinct patterns related to levels of expression. (A) nSSU-rDNA nanochromosomes (red) are found throughout the macronucleus (blue, DAPI; purple, overlay). (B) α-Tubulin chromosomes (green) are also distributed throughout the macronucleus despite lower copy number (blue, DAPI; yellow, overlay). (C) Nanochromosomes of β-tubulin P2 (red) are restricted to the orthomere despite similar copy number to nSSU-rDNA nanochromosomes (blue, DAPI; purple, overlay). (D) Similarly, β-tubulin P3 nano chromosomes (green) are also limited to the orthomere of the macronucleus (blue, DAPI; yellow, overlay). Scale bar: 3 μm.
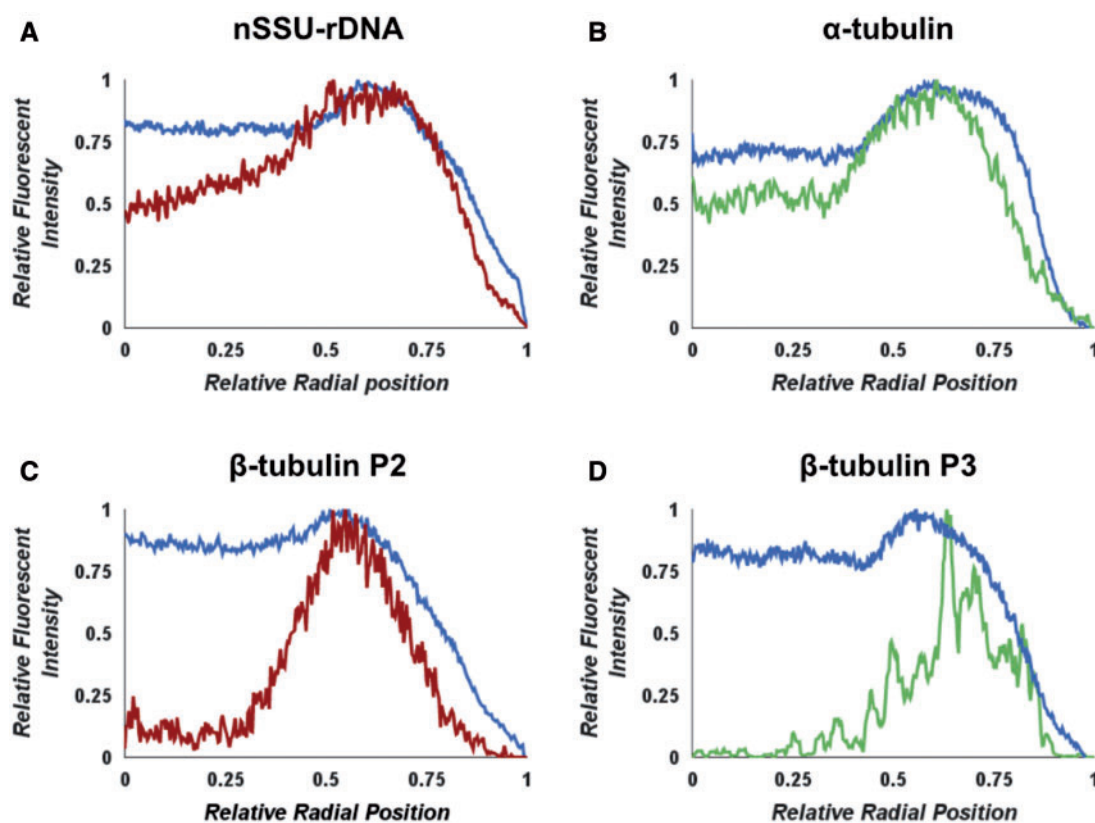
Fig. 3.—Radial distribution of fluorescent intensity of probes in the *Chilodonella uncinata* macronucleus shows distribution of nanochromosomes. Fluorescent intensity of nanochromosomes (red—high copy number *A*, *C*; green—low copy number *B*, *D*) and bulk DNA (blue) are measured along the radius of the macronucleus, from center to the nuclear envelope and at 30° increments. (*A*) nSSU-rDNA; (*B*) α-tubulin; (*C*) β-tubulin P2; (*D*) β-tubulin P3.

accessible for transcription. In contrast, nanochromomes with low expression but high copy number that are enriched in the heterochromatin-rich orthomere may serve a skeletal role, maintaining nuclear shape and volume. This structural role is analogous to the positioning of gene-poor and silent loci of animal and plant chromosomes that form the core of chromosome territories (Fransz et al. 2002; Bickmore and van Steensel 2013) and perhaps also the existence of condensed chromosomes found in interphase in "core dinoflagellates" (Bachvaroff et al. 2014).

Transcriptional Activity Is Related to Degrees of Codon Usage Bias

We assessed the relationship between patterns of genome evolution and gene expression by examining patterns of codon bias of genes from the published transcriptome of *C. uncinata* (Grant et al. 2012). Specifically, we examined the relationship between the GC content at 4-fold degenerate third positions (GC3s) and codon bias (ENc) in 974 protein-coding genes. Estimates of GC3s based on the *C. uncinata* transcriptome show a relatively high average GC content

(53.6%) in protein-coding genes as compared with other ciliates such as *Ichthyophthirius multiformis* (15.9%; Coyne et al. 2011), *T. thermophila* (16.1%; Eisen et al. 2006), *S. lemnae* (23.0%; Aeschlimann et al. 2014), and *Oxytricha trifallax* (24.9%; Swart et al. 2013). The range in GC3s for *C. uncinata* (~30–70%; fig. 4A) is very broad compared with protein-coding genes among other ciliate lineages such as in *T. thermophila* (~10–25%) and in *O. trifallax* (~15–35%), which may be due to the unusual genome architecture in *C. uncinata*. This variance is also reflected in the codon bias of protein-coding genes in *C. uncinata*, ranging from 27 to 61 (fig. 4A).

Despite the large variance in GC content at 4-fold degenerate sites, we found a weaker relationship between codon usage bias and gene expression as compared with *T. thermophila*. To determine this relationship, we examined the correlation between codon usage bias (strength and direction) and expression levels as determined from previous transcriptome data for *C. uncinata* (Grant et al. 2012) and *T. thermophila* (Miao et al. 2009). Using the number of reads from the *C. uncinata* and *T. thermophila* transcriptomes as a proxy for gene expression reveals that genes that are more highly
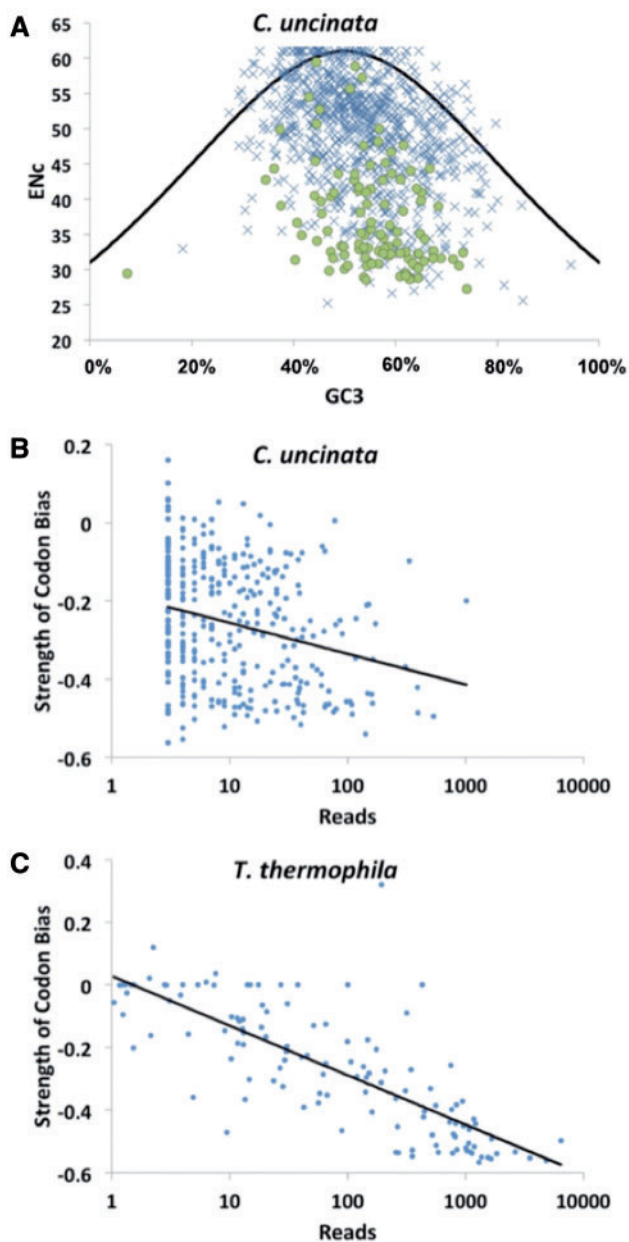
FIG. 4.—Codon bias and gene expression are linked in *Chilodonella uncinata* and *Tetrahymena thermophila*. The strength and direction of codon bias corresponds to gene expression in *C. uncinata* (*A*, *B*) and *Tetrahymena* (*C*). (*A*) Highly expressed genes (green circles) are typified by greater codon bias (lower ENc values) than lowly expressed genes (blue x's). (*B*) Vegetative gene expression in *C. uncinata* is somewhat correlated to the degree of codon bias ($R = -0.261$, $P = 1.262 \times 10^{-6}$). (*C*) Peak gene expression in *Tetrahymena thermophila* is strongly correlated to codon bias ($R = -0.785$, $P \ll 0.05$).

expressed typically have the greatest codon bias, whereas genes with low codon bias appear to be lowly expressed (fig. 4). Transcriptomes of *T. thermophila* have been generated

for all major life stages (asexual growth, starvation, and sexual conjugation). From these data sets, we examined over 100 protein-coding genes from the available transcriptomes of *T. thermophila* focusing on the relationship between peak expression and patterns of codon bias (Miao et al. 2009). Analyses of these genes demonstrate the relationship between peak gene expression and codon bias (fig. 4*C*; $R = -0.785$, $P \ll 0.05$); highly expressed genes have great codon bias. The precise relationship between codon bias in *C. uncinata* and expression is weak (fig. 4*B*; $R = -0.261$, $P = 1.262 \times 10^{-6}$). Unlike *T. thermophila*, transcriptome data for *C. uncinata* are from unsynchronized cultures in which the bulk of cells are vegetative and ~5% are in conjugation; the lack of synchronized cultures in *C. uncinata* may explain the variability in the relationship between codon bias and expression (fig. 4*B*).

Analyses of protein-coding genes in animals (Duret and Mouchiroud 1999; Zhang and Li 2004; Ma et al. 2014), plants (Feng et al. 2013; Amanda et al. 2015), and fungi (Duret and Mouchiroud 1999) have shown that codon usage bias correlates with gene expression for many of genes, where highly expressed genes are the most biased in codon usage (Hershberg and Petrov 2008). Greater codon bias in plants and animals is typical of developmentally important genes, suggesting the increased expression of these genes during brief developmental time periods followed by large periods of decreased expression (Chavez-Barcenas et al. 2000; Schmid et al. 2005). Similarly, we found that numerous conserved proteins (e.g., histones and macronuclear development protein) in *C. uncinata* comprise the fraction of lowly expressed and highly biased genes in the *C. uncinata* transcriptome. Examination of the expression of homologous conserved genes from *T. thermophila* (e.g., histones, elongation factors, epigenetic proteins—DNA methyltransferase) reveal that these genes are often expressed throughout all major life stages, at relatively low levels, undergoing brief periods of intense transcription during specific events, such as conjugation (Miao et al. 2009; Forcob et al. 2014).

Synthesis

Combining analysis of the transcriptome of *C. uncinata* with fluorescence microscopy reveals the following: 1) there exists a distinct organization of *C. uncinata*'s gene-size nanochromosome relative expression levels: highly expressed genes are enriched in the transcriptionally active and DNA-poor paramere of the macronucleus; 2) gene expression is linked to patterns of codon usage bias as protein-coding genes with the greatest bias are more highly expressed; and 3) taken together observed patterns of molecular evolution appear to be intrinsically linked to the nuclear architecture of *C. uncinata*. Our conclusions can be combined with insights from other eukaryotic lineages as highly expressed genes are typically under more evolutionary constraint and have significantly fewer nucleotide
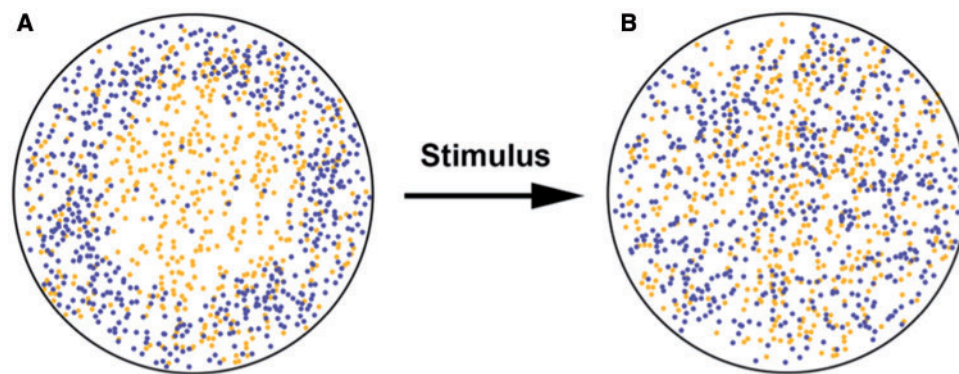
Fig. 5.—We hypothesize the existence of a "gene bank" in *Chilodonella uncinata*, whereby genes that are lowly expressed in vegetative cells are concentrated near the nuclear envelope of the marconucleus; these genes (i.e., nanochromosomes) may move into the center of the nucleus, allowing rapid changes in transcriptional activity in response to environmental and/or developmental cues. (*A*) Transcriptionally active nanochromosomes (orange) are enriched in the nuclear center, while lowly expressed nanochromosomes (blue) are mostly distributed near the nuclear envelope (black) where they comprise the gene bank. (*B*) In response to developmental or environmental cues, previously lowly expressed genes (blue) can quickly move from the gene bank to the transcriptionally active center, resulting in a rapid transition from low to high expression.

substitutions at silent sites, a signatures of codon bias (Duret and Mouchiroud 1999; Hershberg and Petrov 2008; Feng et al. 2013; Amanda et al. 2015). Highly expressed genes are often found in close proximity to chromatin- poor areas or recruited to these areas in numerous eukaryotes, including ciliates (this study; Postberg et al. 2006), dinoflagellates (Figueroa et al. 2014; de la Espina et al. 2005), trypanosomes (Navarro et al. 2007), plants (Fransz et al. 2002; Schubert and Shaw 2011), and animals (Pombo et al. 1997; Mahy et al. 2002; Osborne et al. 2004; Postberg et al. 2006). This interplay between molecular evolution and nuclear architecture may be common to eukaryotes, although it may be more exaggerated in unusual nuclear architectures of lineages such as is found in *C. uncinata*.

We further hypothesize that the heteromeric nuclear architecture in *C. uncinata* provides a "gene bank" (fig. 5). Under this model, the DNA-rich peripheral orthomere harbors the bulk of high copy number nanochromosomes that have low expression in vegetative cells. By having this envelope of nanochromosomes surrounding the transcriptionally active paramere, there may be rapid transitions in transcriptional states by changes in nanochromosome position in response to developmental and environmental cues (fig. 5). Despite occurring at different scales, *C. uncinata*'s "gene bank" shares similarities with the well characterized resting egg banks described in copepods (Metazoa) whereby a large numbers of dormant eggs can remain viable for large periods of time, becoming active during optimal hatching periods (Marcus et al. 1994; Drillet et al. 2011). Just as these animals essentially move from their egg bank to the water column (upon activation), the gene bank in *C. uncinata* consists of inactive chromosomes that can rapidly move into transcriptionally active areas.

Literature Cited

Aeschlimann SH, et al. 2014. The draft assembly of the radically organized *Stylonychia lemnae* macronuclear genome. Genome Biol Evol. 6:1707–1723.

Akhtar A, Gasser SM. 2007. The nuclear envelope and transcriptional control. Nat Rev Genet. 8:507–517.

Bachvaroff TR, et al. 2014. Dinoflagellate phylogeny revisited: using ribosomal proteins to resolve deep branching dinoflagellate clades. Mol Phylogenet Evol. 70:314–322.Bellec L, Katz LA. 2012. Analyses of chromosome copy number and expression level of four genes in the ciliate *Chilodonella uncinata* reveal a complex pattern that suggests epigenetic regulation. Gene 504:303–308.

Bellec L, Maurer-Alcala XX, Katz LA. 2014. Characterization of the life cycle and heteromeric nature of the macronucleus of the ciliate *Chilodonella uncinata* using fluorescence microscopy. J Eukaryot Microbiol. 61:313–316.

Bickmore WA, van Steensel B. 2013. Genome architecture: domain organization of interphase chromosomes. Cell 152:1270–1284.

Chavez-Barcenas AT, et al. 2000. Tissue-specific and developmental pattern of expression of the rice sps1 gene. Plant Physiol. 124:641–653.

Coyne RS, et al. 2011. Comparative genomics of the pathogenic ciliate *Ichthyophthirius multifiliis*, its free-living relatives and a host species provide insights into adoption of a parasitic lifestyle and prospects for disease control. Genome Biol. 12:r100.

Cremer M, et al. 2001. Non-random radial higher-order chromatin arrangements in nuclei of diploid human cells. Chromosome Res. 9:541–567.

de la Espina SMD, Alverca E, Cuadrado A, Franca S. 2005. Organization of the genome and gene expression in a nuclear environment lacking histones and nucleosomes: the amazing dinoflagellates. Eur J Cell Biol. 84:137–149.

De La Torre AR, Lin YC, Van de Peer Y, Ingvarsson P. 2015. Genome-wide analysis reveals diverged patterns of codon bias, gene expression and rates of sequence evolution in picea gene families. Genome Biol Evol. 7:1002–1005.

Diaz-Castillo C, Golic KG. 2007. Evolution of gene sequence in response to chromosomal location. Genetics 177:359–374.

Drillet G, Hansen BW, Kiorboe T. 2011. Resting egg production induced by food limitation in the calanoid copepod *Acartia tonsa*. Limnol Oceanogr. 56:2064–2070.

Duret L. 2002. Evolution of synonymous codon usage in metazoans. Curr Opin Genet Dev. 12:640–649.

Duret L, Mouchiroud D. 1999. Expression pattern and, surprisingly, gene length shape codon usage in Caenorhabditis, Drosophila, Arabidopsis. Proc Natl Acad Sci U S A. 96:4482–4487.

Eisen JA, et al. 2006. Macronuclear genome sequence of the ciliate *Tetrahymena thermophila*, a model eukaryote. PLoS Biol. 4:e286.

Feng C, et al. 2013. Codon usage patterns in Chinese bayberry (*Myrica rubra*) based on RNA-Seq data. BMC Genomics 14:732.

Figueroa RI, Cuadrado A, Stuken A, Rodriguez F, Fraga S. 2014. Ribosomal DNA organization patterns within the dinoflagellate genus Alexandrium as revealed by FISH: life cycle and evolutionary implications. Protist 165:343–363.

Foissner W. 1996. Ontogenesis in ciliated protozoa with emphasis on stomatogenesis. In: Hausmann K, Bradbury PC, editors. Ciliates: cells as organisms. Stuttgart (Germany): Gustav Fisher. p. 95–178.

Forcob S, Bulic A, Jonsson F, Lipps HJ, Postberg J. 2014. Differential expression of histone H3 genes and selective association of the variant H3.7 with a specific sequence class in Stylonychia macronuclear development. Epigenetics Chromatin 7:4.

Fransz P, de Jong JH, Lysak M, Castiglione MR, Schubert I. 2002. Interphase chromosomes in Arabidopsis are organized as well defined chromocenters from which euchromatin loops emanate. Proc Natl Acad Sci U S A. 99:14584–14589.

Grant JR, et al. 2012. Gene discovery from a pilot study of the transcriptomes from three diverse microbial eukaryotes: *Corallomyxa tenera*, *Chilodonella uncinata*, and *Subulatomonas tetraspora*. Protist Genomics 1:3–18.

Hausmann K, Bradbury PC. 1996. Ciliates: cells as organisms. Stuttgart (Germany): Gustav Fischer.

Hershberg R, Petrov DA. 2008. Selection on codon bias. Ann Rev Genet. 42:287–299.

Huang J, Katz LA. 2014. Nanochromosome copy number does not correlate with RNA levels though patterns are conserved between strains of the ciliate morphospecies *Chilodonella uncinata*. Protist 165:445–451.

Kupper K, et al. 2007. Radial chromatin positioning is shaped by local gene density, not by gene expression. Chromosoma 116:285–306.

Ma LN, Cui P, Zhu J, Zhang ZH, Zhang Z. 2014. Translational selection in human: more pronounced in housekeeping genes. Biol Direct. 9:17.

Mahy NL, Perry PE, Bickmore WA. 2002. Gene density and transcription influence the localization of chromatin outside of chromosome territories detectable by FISH. J Cell Biol. 159:753–763.

Marcus NH, Lutz R, Burnett W, Cable P. 1994. Age, viability, and vertical distribution of zooplankton resting eggs from an anoxic basin—evidence of an egg bank. Limnol Oceanogr. 39:154–158.

Meister P, Towbin BD, Pike BL, Ponti A, Gasser SM. 2010. The spatial dynamics of tissue-specific promoters during C-elegans development. Genes Dev. 24:766–782.

Miao W, et al. 2009. Microarray analyses of gene expression during the *Tetrahymena thermophila* life cycle. PLoS One 4:e4429.

Navarro M, Penate X, Landeira D. 2007. Nuclear architecture underlying gene expression in *Trypanosoma brucei*. Trends Microbiol. 15:263–270.

Osborne CS, et al. 2004. Active genes dynamically colocalize to shared sites of ongoing transcription. Nat Genet. 36:1065–1071.

Pombo A, et al. 1997. Transcription factories and chromosome structure. Chromosomes Today 12:147–160.

Postberg J, Alexandrova O, Cremer T, Lipps HJ. 2005. Exploiting nuclear duality of ciliates to analyse topological requirements for DNA replication and transcription. J Cell Sci. 118:3973–3983.

Postberg J, Alexandrova O, Lipps HJ. 2006. Synthesis of pre-rRNA and mRNA is directed to a chromatin-poor compartment in the macronucleus of the spirotrichous ciliate *Stylonychia lemnae*. Chromosome Res. 14:161–175.

Prescott DM. 1994. The DNA of ciliated protozoa. Microbiol Rev. 58:233–267.

Pyne CK. 1978. Electron-microscopic studies on macronuclear development in ciliate *Chilodonella uncinata*. Cytobiologie 18:145–160.

Radzikowski S. 1976. DNA and RNA synthesis in the nuclear apparatus of *Chilodonella cucullus*. Acta Protozool. 15:47–58.

Radzikowski S, Steinbruck G. 1990. Location of rDNA in the heteromeric macronucleus of *Chilodonella steini*. Eur J Protistol. 25:249–254.

Raikov IB. 1982. The protozoan nucleus: morphology and evolution. Vienna (Austria): Springer.

Riley JL, Katz LA. 2001. Widespread distribution of extensive genome fragmentation in ciliates. Mol Biol Evol. 18:1372–1377.

Schmid M, et al. 2005. A gene expression map of *Arabidopsis thaliana* development. Nat Genet. 37:501–506.

Schubert I, Shaw P. 2011. Organization and dynamics of plant interphase chromosomes. Trends Plant Sci. 16:273–281.

Simonis M, et al. 2006. Nuclear organization of active and inactive chromatin domains uncovered by chromosome conformation capture-on-chip (4C). Nat Genet. 38:1348–1354.

Straatman KR, Trompetter CM, Schul W, Schel JHN. 1996. Fluorescent labelling of nascent RNA reveals nuclear transcription domains throughout plant cell nuclei. Protoplasma 192:145–149.

Sun HB, Shen J, Yokota H. 2000. Size-dependent positioning of human chromosomes in interphase nuclei. Biophys J. 79:184–190.

Swart EC, et al. 2013. The *Oxytricha trifallax* macronuclear genome: a complex eukaryotic genome with 16,000 tiny chromosomes. PLoS Biol. 11:e1001473.

Tai PWL, et al. 2014. The dynamic architectural and epigenetic nuclear landscape: developing the genomic almanac of biology and disease. J Cell Physiol. 229:711–727.

Tanabe H, Habermann FA, Solovei I, Cremer M, Cremer T. 2002. Non-random radial arrangements of interphase chromosome territories: evolutionary considerations and functional implications. Mutat Res. 504:37–45.

Zhang LQ, Li WH. 2004. Mammalian housekeeping genes evolve more slowly than tissue-specific genes. Mol Biol Evol. 21:236–239.

Zwirglmaler K, Ludwig W, Schleifer KH. 2003. Improved fluorescence in situ hybridization of individual microbial cells using polynucleotide probes: the network hypothesis. Syst Appl Microbiol. 26:327–337.

Associate editor: Rebecca Zufall